J Neurophysiol 95: 76–87, 2006.
First published September 28, 2005; doi:10.1152/jn.00624.2005.

Hyperpolarization-Activated Currents Regulate Excitability in Stellate Cells of the Mammalian Ventral Cochlear Nucleus

Aldo Rogelis A. Rodrigues, and Donata Oertel
Department of Physiology, University of Wisconsin, Madison, Wisconsin

Submitted 15 June 2005; accepted in final form 26 September 2005

Rodrigues, Aldo Rogelis A. and Donata Oertel. Hyperpolarization-activated currents regulate excitability in stellate cells of the mammalian ventral cochlear nucleus. *J Neurophysiol* 95: 76–87, 2006. First published September 28, 2005; doi:10.1152/jn.00624.2005. The differing biophysical properties of neurons the axons of which form the different pathways from the ventral cochlear nucleus (VCN) determine what acoustic information they can convey. T stellate cells, excitatory neurons the axons of which project locally and to the inferior colliculus, and D stellate cells, inhibitory neurons the axons of which project to the ipsi- and contralateral cochlear nuclei, fire tonically when they are depolarized, and, unlike other cell types in the VCN, their firing rates are sensitive to small changes in resting currents. In both types of neurons, the hyperpolarization-activated current (I_h) reversed at −40 mV, was activated at voltages negative to −60 mV, and half-activated at approximately −88 mV; maximum hyperpolarization-activated conductances ($g_{h\ max}$) were 19.1 ± 2.3 nS in T and 30.3 ± 2.6 nS in D stellate cells (means ± SE). Activation and deactivation were slower in T than in D stellate cells. In both types of stellate cells, 50 μM 4(*N*-ethyl-*N*-phenylamino)1,2-dimethyl-6-(methylamino) pyridinium chloride (ZD7288) and 2 mM Cs^+ blocked a 6- to 10-fold greater conductance than the voltage-dependent g_h determined from Boltzmann analyses at −62 mV. The voltage-insensitive, ZD7288-sensitive conductance was proportional to $g_{h\ max}$ and g_{input}. 8-Br-cAMP shifted the voltage dependence of I_h in the depolarizing direction, increased the rate of activation, and slowed its deactivation in both T and D stellate cells. Reduction in temperature did not change the voltage dependence but reduced the maximal g_h with a Q_{10} of 1.3 and slowed the kinetics with a Q_{10} of 3.3.

INTRODUCTION

Hyperpolarization-activated cation currents (I_h) perform a wide range of functions in excitable cells. In many neurons, I_h contributes to setting the resting potential (Bal and Oertel 2000; Banks et al. 1993; Doan and Kunze 1999; Pape 1996) and to controlling the rate of spontaneous and evoked firing (Maccaferri and McBain 1996; McCormick and Pape 1990b; Spain et al. 1987). In hippocampal cells, I_h contributes to synaptic integration in dendrites (Magee 1998; Williams and Stuart 2000). These functions can be modulated through cAMP-mediated signaling pathways (Cathala and Paupardin-Tritsch 1999; DiFrancesco and Tortora 1991; Ingram and Williams 1996; Ludwig et al. 1998; McCormick and Pape 1990a; Pedarzani and Storm 1995; Saitow and Konishi 2000; Tokimasa and Akasu 1990; van Ginneken and Giles 1991; Vargas and Lucero 1999).

The shapes, projections, and biophysical characteristics of the four groups of principal cells of the VCN, bushy, octopus, T stellate, and D stellate cells, are distinct. Octopus cells occupy the most caudal and dorsal VCN in a sharply delineated area (Golding et al. 1995). The remainder of the VCN contains intermingled bushy and stellate cells with bushy cells being more common anteriorly and stellate cells more common posteriorly. The low input resistances that result from the activation of g_h and a low-voltage activated K^+ conductance, g_{KL}, make responses to synaptic currents in octopus and bushy cells fast and precisely timed, and responses to current pulses transient (Bal and Oertel 2000; Cuttle et al. 2001; Manis and Marx 1991; Oertel et al. 2000). The absence (or near absence) of g_{KL} in stellate cells allows them to fire tonically when they are depolarized; their rates of firing are sensitive to small changes in resting currents (Ferragamo and Oertel 2002; Fujino and Oertel 2001; Oertel et al. 1990). The responses of VCN cells to sound have been shown in vivo to be sensitive to neuromodulation (Kossl and Vater 1989).

Two types of stellate cells have been distinguished and named on the basis of several differences. In slices from mice, they were named for their projection patterns. Both types project locally in the ventral and dorsal cochlear nuclei but the main axon projects through the Trapezoid body in T stellate cells but Dorsalward through the intermediate acoustic stria in D stellate cells (Oertel et al. 1990). Other authors have distinguished T and D stellate cells on the basis of other differences: "type 1" and "type 2" vary in the degree of somatic inputs in electron micrographs (Cant 1981), responses to tones are "chopper" or more transient "onset-chopper" (Blackburn and Sachs 1989; Smith and Rhode 1989), the dendrites of "planar" stellate cells are aligned with auditory nerve fibers, whereas those of "radial" stellate cells are not (Doucet and Ryugo 1997). T stellate cells are glutamatergic and form a major excitatory pathway to the contralateral inferior colliculus (Adams and Warr 1976), whereas D stellate cells are glycinergic and inhibitory (Ferragamo et al. 1998; Needham and Paolini 2003). Many, but probably not all, D stellate cells project to the contralateral cochlear nuclei (Arnott et al. 2004; Cant and Gaston 1982; Needham and Paolini 2003). T stellate cells are narrowly tuned and fire tonically in responses to tones, whereas D stellate cells are more broadly tuned and fire transiently at the onset of tones (Arnott et al. 2004; Blackburn and Sachs 1989; Jiang et al. 1996; Nelken and Young 1994; Palmer and Winter 1996; Palmer et al. 1996; Smith and Rhode 1989; Smith et al. 2005).

The present experiments show that g_h regulates the firing of stellate cells through its influence on the resting potential and input resistance. The sensitivity of g_h to cAMP levels indicates that firing in both types of stellate cells can be regulated

Address for reprint requests and other correspondence: D. Oertel, Dept. of Physiology, University of Wisconsin Medical School, 1300 University Ave., Madison, WI 53706 (E-mail: oertel@physiology.wisc.edu).

The costs of publication of this article were defrayed in part by the payment of page charges. The article must therefore be hereby marked "*advertisement*" in accordance with 18 U.S.C. Section 1734 solely to indicate this fact.

neuronally. We were surprised to discover in the course of our analysis that ZD7288 and extracellular Cs^+, drugs that are commonly used to block g_h, block more than the voltage-sensitive g_h.

METHODS

Preparation of slices

All experiments were done in accordance with the guidelines of the Research Animal Resources Center at the University of Wisconsin-Madison. Parasagittal slices were prepared from the cochlear nuclei of ICR mice between 16 and 18 days old. During the surgery, the auditory nerve was cut where it exits the internal auditory meatus. A block of brain tissue containing the cochlear nucleus was trimmed and glued onto a Teflon-coated specimen disc. The slices (200 μm thick) were prepared with a VT1000S oscillating tissue slicer (Leica, Nussloch, Germany) using a sapphire blade (Delaware Diamonds Knives, Wilmington, DE). The tissue was kept submerged in physiological saline of the following composition (mM): 127 NaCl, 3 KCl, 1.2 KH_2PO_4, 2.4 $CaCl_2$, 1.3 $MgSO_4$, 3 HEPES, 20 $NaHCO_3$, and 10 glucose, pH 7.4 when saturated with 95% O_2-5% CO_2 at 26°C. The osmolality, measured with a 3D3 Osmometer (Advanced Instruments, Norwood, MA), was 302 mOsm/kg. Slices were transferred to a recording chamber (~0.6 ml) and superfused continually at 5–6 ml/min. The temperature of the inflowing perfusate was monitored with a small thermistor, IT-23, and a Thermalert thermometer TH-5 (Physitemp, Clifton, NJ) and kept at 33 ± 0.5°C in most of the experiments by a custom-built, feedback-controlled heater. The recording chamber was placed on the stage of an Axioskop 2FS microscope (Zeiss, Oberkochen, Germany) and individual neurons were visualized using differential interference contrast optics (×63/0.9 w water-immersion lens).

Electrophysiological recordings

Patch pipettes were made from borosilicate glass capillaries (1B120F-4, World Precision Instruments) and had resistances of between 3.8 and 5 MΩ when filled with a solution containing (in mM) 110 potassium gluconate, 9 HEPES, 9 EGTA, 4.5 $MgCl_2$, 14 phosphocreatinine, 0.3 GTP, and 4 Na_2ATP, pH 7.3 (KOH), 293 mOsm/kg. In normal extracellular saline, this solution yielded a junction potential of −12 mV that was added to all voltages. Whole cell current- and voltage-clamp recordings were performed with an Axopatch 200B amplifier controlled by a PC computer through a Digidata 1200 computer interface and pClamp 8.0 software (Axon Instruments, Foster City, CA). The access resistance (R_a) was monitored throughout all experiments and ranged from 9 to 17 MΩ. R_a was partially compensated on-line between 60 and 75% with a 20-μs lag time. For analysis of the voltage dependence of activation, the voltage drop caused by the uncompensated R_a was subtracted off-line from the applied voltage command to yield a precise value of transmembrane voltage (Rothman and Manis 2003). Voltage responses to current injection and current responses to voltage steps were recorded at 40 and 5 kHz and filtered at 10 and 1 kHz, respectively.

Data analysis

The input resistance (R_{input}) was determined in a subset of cells from the slope of the relationship between the mean voltage responses in three consecutive recordings to the last 50 ms of 300-ms current pulses from −60 to +60 pA in 10-pA steps. To achieve the greatest possible accuracy in these measurements, the voltage drop across the access resistance was subtracted (bridge was balanced) off-line in the following way. The 0.2 ms after the end of the current pulse that was contaminated by electrode artifacts was eliminated and reconstructed by fitting the time course of decay after the offset with a single exponential and extrapolating back to the offset of the current pulse. Activation and deactivation time constants of I_h were determined by fitting the current evoked during an activating or deactivating pulse to double exponential functions of the form: $I_h(t) = I_{SS} + A_f e^{-t/\tau_f} + A_s e^{-t/\tau_s}$ where $I_h(t)$ is the current at time t, I_{SS} is the steady state current, A_f and A_s are the initial amplitudes of the fast (τ_f) and slow (τ_s) exponential components, respectively. To avoid contamination by the capacitative artifacts, the first 12 to 15 ms of the recorded current were not included in the fit. The voltage sensitivity of g_h was measured from tail currents. The amplitude of individual tail currents, measured 12 ms after the end of the conditioning step (I), was normalized as a function of maximal and minimal tail currents as $I(V) = (I - I_{min})/(I_{max} - I_{min})$ and plotted as a function of the voltage of the preceding step (V) and reflects the relative conductance (g). Each of the measurements from individual cells was fitted by a Boltzmann function of the form: $g(V) = 1/1 + e^{[(V - V_{0.5})/k]}$ from which the value of half-maximal activation voltage ($V_{0.5}$) and the slope factor (k) were derived. The maximal conductance ($g_{h\ max}$) was determined from tail currents using the Ohm's law $g = (I_{max} - I_{min})/(V - V_{rev})$, where I_{max} was the tail current after a fully activating voltage step, I_{min} was the tail current after a step to −52 mV, V was the voltage at which the tail currents were measured (−77 mV), and V_{rev} the reversal potential of I_h. The Q_{10} for the change in $g_{h\ max}$ and kinetics of activation was determined from the relationship: $Q_{\Delta T} = (Q_{10})^{\Delta T/10}$. Data are expressed as means ± SE. Statistical significance was determined using Student's t-test; data were considered significant when the probability of the null hypothesis was <0.05. Measurements were initially analyzed with Clampfit 9.0 (Axon Instruments) and all the plots, fits and statistics were performed with Origin 7.5 (Microcal, Northampton, MA) software.

Chemicals

All measurements of I_h under voltage-clamp were made after blocking other currents pharmacologically. Glycinergic and glutamatergic synaptic currents were blocked with 0.5 μM strychnine and 40 μM 6,7-dinitroquinoxaline-2,3(1H,4H)-dione (DNQX). Voltage-sensitive Na^+ and K^+ currents were blocked with 1 μM tetrodotoxin (TTX) and 2 mM 4-aminopyridine (4-AP). All drugs were added to the saline solution and applied in the bath. In some other recordings, I_h was blocked with 50 μM 4(*N*-ethyl-*N*-phenylamino)1,2-dimethyl-6-(methylamino) pyridinium chloride (ZD7288) or with 2 mM CsCl. Most drugs and reagents were purchased from Sigma (St. Louis, MO), ZD7288 was obtained from Tocris (Bristol, UK) and TTX from Alomone Labs (Jerusalem, Israel).

RESULTS

The following results are based on whole cell patch-clamp recordings from 120 T and 15 D stellate cells in the VCN in which the access resistance, input resistance, and resting potential remained stable throughout the recording. Our sample of recordings from T stellate cells is larger than that of D stellate cells because there are more of them in the VCN. The electrophysiological distinctions between T and D stellate cells are illustrated in Fig. 1. While both T and D stellate cells responded to depolarizing current pulses with sustained firing, the repolarization after action potentials in responses to depolarizing current and the rectification of responses to hyperpolarizing current were subtly different (Ferragamo et al. 1998; Fujino and Oertel 2001; Oertel et al. 1990). In both groups of cells, repolarizing currents associated with the action potential caused a fast and pronounced voltage undershoot (Fig. 1, *). Unlike T stellate cells, repolarization in D stellate cells exhibited an additional slower and more variable undershoot (Fig. 1,

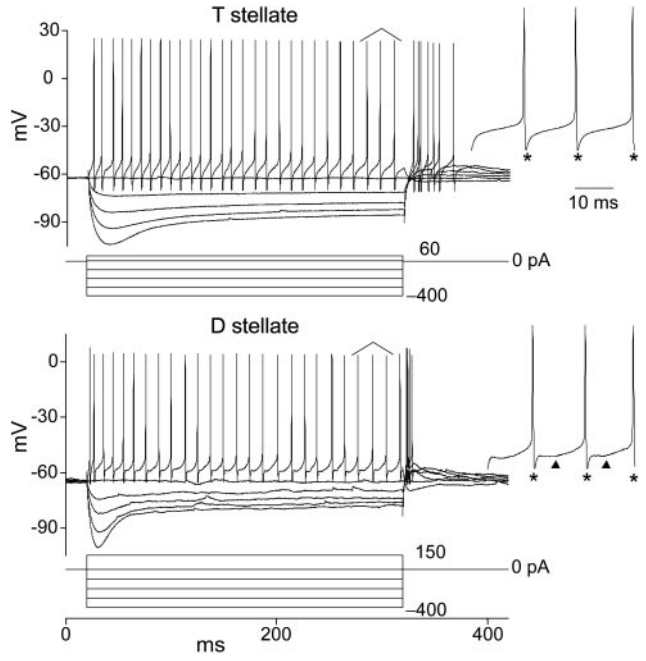

FIG. 1. Responses to somatic current injection in a T and a D stellate neuron. Current pulses evoked hyperpolarizations that were initially large and then sagged back toward rest. In T stellate neurons, the sag was slower and of smaller magnitude than in D stellate cells. Depolarizing current pulses evoked suprathreshold depolarizations that caused steady firing in both types of neurons. The input resistances were 63 MΩ in the T and 68 MΩ in the D stellate neuron. Differences in the shapes of action potentials that contributed to the identification of neurons are illustrated at an expanded time scale in the *insets* (position in the train indicated). In T stellate cells, recovery from the undershoots after action potentials (*) was monotonically rising whereas in D stellate neurons some action potentials were followed by two distinct hyperpolarizations (*, ▲). As is typical, occasional spontaneous synaptic events were observed in both types of neurons; their pharmacological blockade did not affect the observations of undershoots. Recordings were made in normal physiological saline.

bottom, ▲). In response to injection of hyperpolarizing current, voltages fell to a hyperpolarizing peak and then sagged back toward rest. Experiments described below indicate that the sag results from the activation of I_h. The sag was slower and smaller in T stellate than in D stellate cells (Fujino and Oertel 2001). Rebound action potentials after the end of a hyperpolarizing current step were common in both types of cells.

The resting potentials and input resistances of T and D stellate neurons in the absence of any ion channel blockers were not significantly different. The resting potentials were -64.4 ± 0.8 mV ($n = 22$) in T stellate and -64.8 ± 0.4 mV ($n = 13$) in D stellate cells. In a subset of cells, responses were measured to small (10 pA) steps of current in triplicate as described in METHODS. In this sample of cells, the input resistances around rest (R_{input}) had a mean of 74 ± 11 MΩ ($n = 12$) in T stellate and 60 ± 5 MΩ ($n = 11$) in D stellate cells.

Isolation and estimation of I_h

To examine I_h, recordings were made in voltage clamp. It is unlikely that stellate cells are isopotential under voltage clamp because they have long, tapering dendrites and long segments of axons in slices (Oertel et al. 1990). In clamping these cells at depolarized potentials, escaped action potentials were often observed in the absence of Na^+ channels blockers. Outward currents exceeded 12 nA at +10 mV but were unlikely to be clamped well because plots of the instantaneous component of the tail current versus the voltage were not linear and in some cells repeated voltage steps evoked inconsistent current responses. Responses to hyperpolarizing voltages were, however, generally stable under voltage clamp. One interpretation of these observations is that the majority of g_h is located electrically near the recording site and that depolarization-activated g_K and g_{Na} are often located more distantly on axons or other fine processes.

After recording the responses to current pulses in current-clamp mode in the absence and presence of synaptic blockers, 1 μM TTX was added to the physiological saline to block Na^+ currents. Figure 2 shows voltage-clamp recordings of I_h in a T and a D stellate cell when the voltage was stepped from a holding potential of –62 mV to voltages between –57 and –117 mV. Shifts in voltage elicited an instantaneous current (I_{inst}) followed by a slowly developing I_h (Fig. 2*A*). The capacitative current at the onset of a voltage step lasted 6–10 ms. To avoid distortion of I_{inst} by the capacitative artifact, I_{inst} was measured as the mean value of the current over 1 ms centered 12 ms after the onset of steps to between –57 to –77 mV. For larger hyperpolarizing steps, the first 12 ms were excluded, and I_{inst} was measured by fitting the activation of the current with a double-exponential function and extrapolating back to the onset of the step. To isolate I_h, recordings were made in the presence of 2 mM 4-AP. Figure 2*B* shows that 2 mM 4-AP reduced I_{inst}, perhaps as a result of blocking a small, low-voltage activated K^+ current (I_{KL}) (Rothman and Manis 2003).

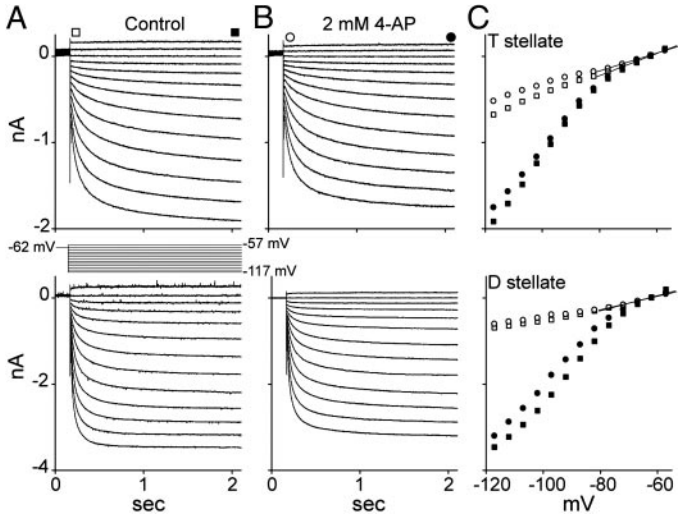

FIG. 2. Sensitivity of stellate neurons to 4-aminopyridine (4-AP). *A*: voltage-clamp recordings in a T (*top*) and a D (*bottom*) stellate neuron. From −62 mV, voltage pulses to between –57 and –117 in 5-mV steps elicited an instantaneous and a slowly activating, inward current, I_h. In control recordings, 40 μM 6,7-dinitroquinoxaline-2,3(1H,4H)-dione (DNQX), 0.5 μM strychnine, and 1 μM TTX were added to the bath. To visualize the instantaneous currents, only the first 2 s of responses to 3-s voltage pulses are illustrated. *B*: adding 2 mM 4-AP reduced the amplitude of the instantaneous and steady-state currents. *C*: plots show the instantaneous current (○, □), measured 12 ms after the beginning of the voltage pulses (–57 to –72 mV) or by extrapolating the exponential fits to t = 0 (–77 to –117 mV), and steady-state current (●, ■), measured at the end of the pulse. The slopes of the relationships between instantaneous current and voltage are a measure of the cells' input conductance. 4-AP reduced the input conductance at –62 mV from 12.9 to 10.4 nS in the T stellate cell and from 17.7 to 15.8 nS in the D stellate cell.

In some cells, the plot of I_{inst} versus the applied voltage deviated from linearity in the absence of 4-AP, causing measurements of the input conductance (g_{input}) (slope) to depend on the range of voltages over which the slope was fit. The g_{input} at −62 mV was therefore estimated from linear fits of I_{inst}-V plots between −57 and −77 mV (Fig. 2*C*). Adding 2 mM 4-AP decreased the slope and made I_{inst} a more linear function of voltage. In the T and D stellate neurons shown in Fig. 2*C*, the g_{input} decreased from 12.9 to 10.4 nS and from 17.7 to 15.8 nS, respectively. On average, in the presence of 2 mM of 4-AP, the g_{input} was 12.0 ± 1.3 nS (n = 16) in T stellate cells and 12.4 ± 1.2 nS (n = 6) in D stellate cells. Adding 4-AP reduced g_{input} by 19.4 ± 4.6% (n = 6) in T stellate and by 17.8 ± 3.8% (n = 5) in D stellate cells. To determine whether 4-AP affects I_h, I_h was first separated from other currents by subtracting I_{inst} from the current evoked by a voltage step from −62 to −92 mV (not shown). I_h was reduced by 18.4% (n = 8) on average in T stellate and by 14.4% (n = 3) in D stellate cells by 2 mM 4-AP.

Reversal potential of I_h

The reversal potentials were measured from the intersection in I_{inst}-V plots after conditioning pulses to three different voltages. Figure 3 illustrates how the measurement of the reversal potential for I_h was made in a D stellate cell. I_h was activated by hyperpolarizing, conditioning pulses to three different voltages (Fig. 3*A*). Pulses were longer for the smaller hyperpolarizations to allow currents to approach the steady state. Plots of I_{inst} 12 ms after the end of the conditioning pulses were linear as a function of the voltage with the slopes reflecting the magnitude of the previous, steady-state conductance (Fig. 3*B*). At the reversal potential, no current flows through g_h so that I_h is equal (0 nA) under all conditions. The reversal potential was measured as the point at which the regression lines, fitted to the I_{inst}-V relationships, intersect. Reversal potentials in T stellate cells were −40 ± 2 mV (n = 6), those in D stellate cells were −41 ± 4 mV (n = 4) (Fig. 3*C*). The I_{inst}-V relationships were linear and intersected at one point, indicating that g_h was reasonably well space-clamped.

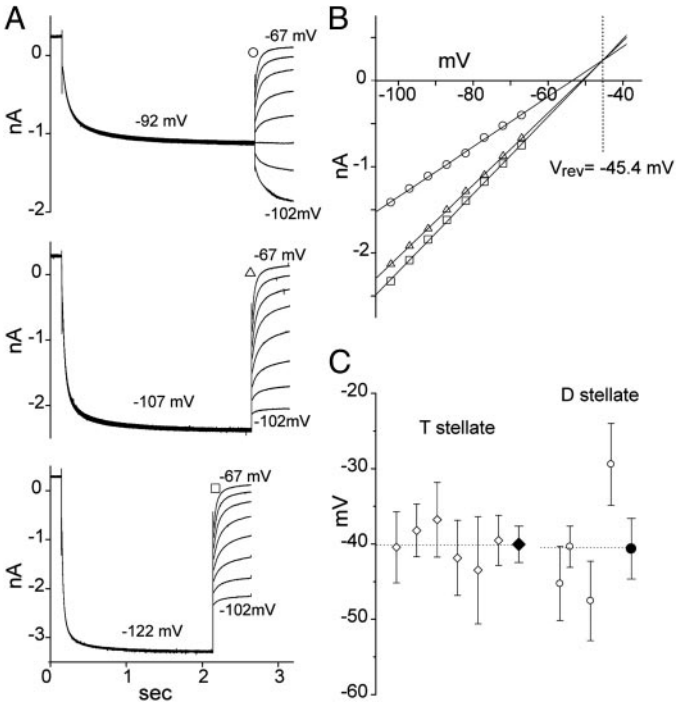

FIG. 3. Estimate of the reversal potential of I_h in a D stellate cell. *A*: conditioning pulses long enough for currents to reach steady-state levels to 3 conditioning potentials (–92, –107, and –122 mV) activated I_h. The instantaneous current after the end of the conditioning pulses (symbols) reflected a voltage-dependent g_h and a voltage-independent leakage conductance. *B*: instantaneous currents following the conditioning pulses are plotted as a function of the test potential. For each conditioning voltage, the instantaneous currents were linear functions of voltage the slopes of which reflected the conductance at the end of the conditioning pulse. At the intersection of the 3 regression lines (· · ·), I_h is equal to 0 under each of the 3 conditions, and thus is the reversal potential of I_h. *C*: reversal potentials were measured for 6 T stellate and 4 D stellate cells (◇, ○). On average the reversal potentials of I_h lay at −40 mV in both T and D stellate cells (◆, ●).

Voltage sensitivity and maximum amplitude of g_h

Tail currents were used to measure the voltage sensitivity and maximum amplitude of g_h. The steady-state activation of g_h is reflected in the amplitude of tail currents on return to −77 mV after steps to voltages between −52 to −132 mV (Fig. 4). The tail currents measured at the test voltage (–77 mV) result from the activation or deactivation of I_h after the end of the conditioning pulse. Over the depolarizing voltage range where little or no g_h was activated by the conditioning pulse, the step to –77 mV caused activation of g_h; when the variable voltage pulse was strongly hyperpolarizing, the step to –77 mV caused g_h to be deactivated (Fig. 4*A*). The relative amplitudes of tail currents between the two extremes are a measure of the voltage sensitivity of g_h. The relationship of the normalized conductance as a function of voltage is shown for seven T stellate and eight D stellate cells in Fig. 4*B*. Half-maximal activation of g_h occurred at −88.9 ± 0.7 mV in T stellate and −86.8 ± 1.2 mV in D stellate cells and were not significantly different. The slope factors (k) that reflect the steepness of the relation between voltage and fractional activation of I_h, were 7.8 ± 0.6 and 6.6 ± 0.2 mV in T and D stellate cells, respectively, and were not significantly different. The Boltzmann relationships indicate that only a small fraction of $g_{h\ max}$ is activated at the resting potential, on average 4.1 and 4.5% of the maximal g_h in T and D stellate neurons respectively (Fig. 4*B*). To test whether measurements of the voltage sensitivity might have been distorted by the failure of conditioning pulses to allow the activation of currents to reach the steady state, g_h-V curves generated from tail currents after 3-s pulses and from responses to pulses that varied from 3 to 6.2 s in a T stellate cell were compared. Differences were minimal (Fig. 4*C*). The slope factor differed significantly in T stellate cells when measurements were made with 2- and 3-s pulses, however (data not shown).

Pharmacological block by ZD7288 and Cs^+

In other cells, ZD7288 (BoSmith et al. 1993; Gasparini and DiFrancesco 1997; Harris and Constanti 1995) and Cs^+ (Harris and Constanti 1995; Magee 1998; McCormick and Pape 1990b) have been shown to block I_h. We examined the sensitivity of the currents activated from a holding potential of −62 mV to 50 μM ZD7288. In both T and D stellate cells, ZD7288 blocked I_h almost completely, and it significantly reduced I_{inst}

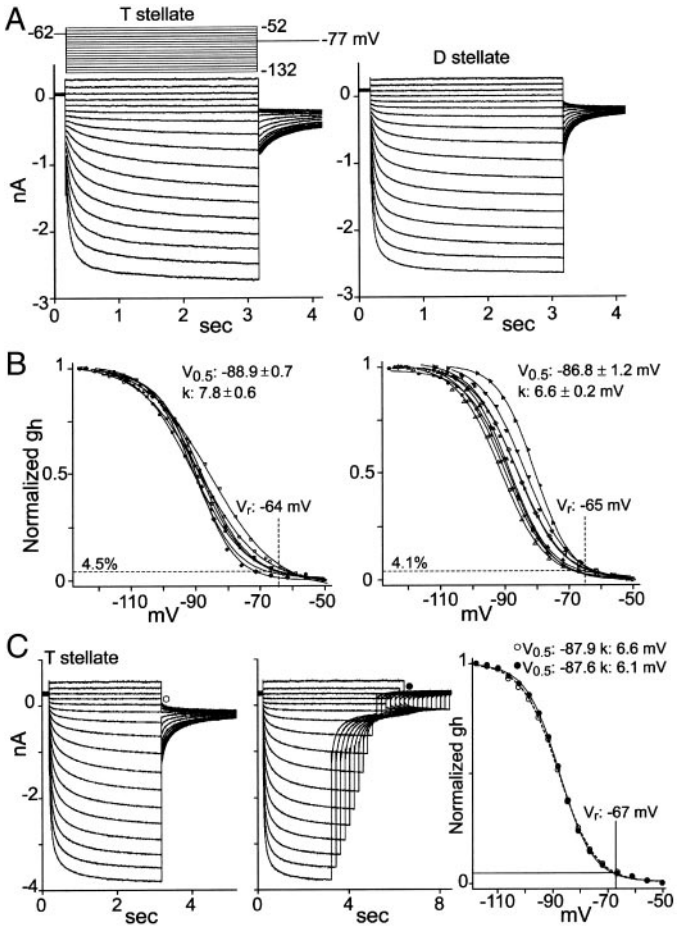

FIG. 4. Voltage sensitivity of g_h in T stellate and D stellate neurons. *A*: voltage was held at −62 mV, then stepped to conditioning pulses between −52 to −132 mV for 3 s, and taken to the test voltage, −77 mV, where the driving force for K^+ was small and where voltage-dependent inward currents are minimally activated. *B*: plots of the normalized tail currents (measured 12 ms after the beginning of the test pulse) as a function of the voltage of the conditioning pulse. The voltage was corrected for uncompensated access resistance and therefore differs slightly from the command voltage shown in *A*. Each cell's (7 T stellate, 7 D stellate cells) measurements were fit with a Boltzmann distribution. At the resting potential (V_r), g_h was activated to 4.5% in T stellate and 4.1% in D stellate cells. *C*: to test whether g_h-*V* relationships were distorted because slowly activating currents had not reached steady state in a T stellate cell, g_h-*V* curves determined from constant 3-s pulses (*left*) were compared with measurements when the duration of pulses was varied so that the slowest pulses were the longest (*middle*). The g_h-*V* plots were almost identical (*right*) indicating that the duration of pulses was long enough to obtain a good representation of the voltage sensitivity of g_h. At the resting potential of this cell (−67 mV) the fractional activation of g_h was 0.047 for the longer pulses and 0.040 for the shorter pulses.

(Fig. 5, *A* and *B*). In responses to strongly hyperpolarizing voltages, some unblocking of ZD7288 occurred with time as has also been observed in other types of neurons (Harris and Constanti 1995; Shin et al. 2001). The I_{inst}-*V* plot shows that g_{input} at −62 mV in the T stellate cell was reduced from 10.4 to 4.4 nS and in the D stellate cell from 10.1 to 6.1 nS (Fig. 5*C*). On average, 50 μM ZD7288 reduced the g_{input} by 49.4 ± 3.1% (n = 11) in T and by 46.2 ± 3.1% (n = 3) in D stellate neurons. The sensitivity to Cs^+ was determined in a similar way. Figure 5 illustrates that 2 mM Cs^+ blocked a substantial proportion of I_h in a T stellate cell. Strong hyperpolarizing pulses revealed that a small, hyperpolarization-activated current remained in the presence of Cs^+, however, indicating that the block by 2 mM Cs^+ was not complete. The g_{input} at −62 mV in this cell was reduced from 10.0 to 8.2 nS. On average, 2 mM Cs^+ reduced g_{input} in T stellate cells by 13.2 ± 3.5% (n = 7). The block by 2 mM Cs^+ in T stellate cells was significantly smaller than that by 50 μM ZD7288.

Voltage-insensitive, ZD7288-sensitive conductance

A goal of the present experiments was to understand how g_h contributes to regulating the excitability of stellate cells and how it contributes to the setting of the resting potential. The large differences, even within an individual cell, of estimates of g_h near rest made from the Boltzmann function, and sensitivity of the input conductances near rest to ZD7288 and Cs^+ prompted a quantitative analysis of conductances near rest.

Measurements were made of $g_{h\ max}$ and g_{input} as described in the preceding text. Maximal g_h was 19.1 ± 2.3 nS (n = 16) in T and 30.3 ± 2.6 nS (n = 6) in D stellate cells (Fig. 6*A*), and the two were significantly different. All recordings that form the basis of this analysis of conductances at −62 mV were

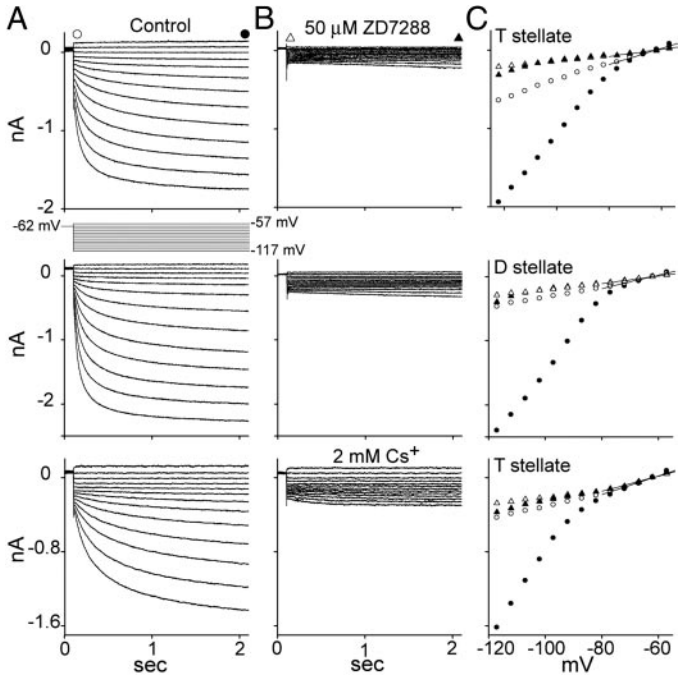

FIG. 5. Effects of 4(*N*-ethyl-*N*-phenylamino)1,2-dimethyl-6-(methylamino) pyridinium chloride (ZD7288) and Cs^+ on the instantaneous and time-dependent currents in T and D stellate cells. *A*: voltage-clamp recordings of I_h in T (*top* and *bottom*) and a D (*middle*) stellate neurons. From −62 mV, voltage pulses elicited an instantaneous and a slowly activating, inward current, I_h. In control recordings, 2 mM 4-AP, 40 μM DNQX, 0.5 μM strychnine, and 1 μM TTX were added to the bath. To visualize the instantaneous currents, only the first 2 s of responses to 3-s voltage pulses are illustrated. *B*: adding 50 μM ZD7288 or 2 mM Cs^+ reduced the amplitude of the instantaneous current and reduced I_h. In the presence of ZD7288 there was some unblocking at strongly hyperpolarized voltages. In the presence of 2 mM Cs^+, some activation of I_h was observed, indicating that the block was incomplete. *C*: plots show the relationship between voltage and the instantaneous (○, △) and steady-state currents (●, ▲). In the T stellate cell, the maximum g_h of which was 23.2 nS, the input conductance at −62 mV was reduced from 10.4 to 4.4 nS by ZD7288. In the D stellate cell, the maximum g_h of which was 30.2 nS, the input conductance was reduced from 10.1 to 6.1 nS, by ZD7288. *Bottom*: Cs^+ reduced the input conductance from 10.0 to 8. 2 nS in the T stellate neuron the maximum g_h of which was 16.8 nS.

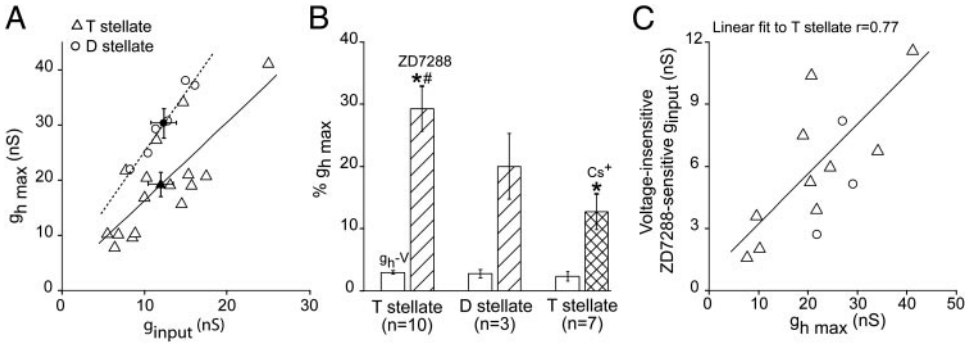

FIG. 6. Relationship of the voltage-dependent g_h and the conductances sensitive to ZD7288 or Cs^+ at −62 mV in T and D stellate cells. All the measurements were made in the presence of 2 mM 4-AP. *A*: plots of $g_{h\ max}$ as a function of g_{input} indicate that the 2 variables are linearly associated. ● and ▲ indicate the means ± SE. *B*: percentage of $g_{h\ max}$ active at −62 mV (□) was determined as illustrated in Fig. 4. The magnitude of the conductance at −62 mV that is sensitive to ZD7288 or Cs^+ is expressed as percentage of $g_{h\ max}$ (▨) in the same sample of cells. In both T and D stellate cells, ZD7288 and Cs^+ block a significantly (*) larger conductance than the proportion of $g_{h\ max}$ than is expected to be active at this voltage from the analysis of the voltage dependence of g_h. The ZD7288-sensitive conductance is also significantly larger than the Cs^+-sensitive conductance (#). *C*: magnitude of the voltage-insensitive, ZD7288-sensitive conductance (the ZD7288-sensitive conductance − g_h at −62 mV) was plotted as a function of $g_{h\ max}$ for 10 T stellate (△) and 3 D stellate cells (○). A regression line fit to the T stellate cell data indicates a positive correlation in the data set (coefficient $r = 0.77$, $P = 0.0023$).

made in the presence of 2 mM 4-AP. Correcting for the fraction of g_h that was blocked by 4-AP, $g_{h\ max}$ were 23.4 nS for T and 35.4 nS for D stellate cells.

There was considerable variability in the g_{input} and $g_{h\ max}$ among recorded neurons. This might be expected if recordings were made from stellate cells the processes of which were cut to varying degrees in the making of slices. We therefore plotted $g_{h\ max}$ as a function of g_{input} and found that they covaried and that the T and D stellate cells with the largest g_{input} also had the largest $g_{h\ max}$ (Fig. 6*A*).

Figure 6*B* shows a comparison of the estimates of g_h active at −62 mV derived from the Boltzmann functions and those derived from pharmacological sensitivity to 50 μM ZD7288 and 2 mM Cs^+. In every T and D stellate cell for which measurements were made, the measurement of the voltage-sensitive g_h was smaller than the conductances blocked by ZD7288 and Cs^+ at −62 mV. Distortions in the Boltzmann function are unlikely to have been large enough to account for these differences. One explanation for these results is that ZD7288 and Cs^+ are not specific for g_h and that each blocks other, unidentified conductances. Such an explanation cannot be excluded but there is a more interesting possibility.

It has recently been demonstrated that in an expression system, the expression of g_h is associated with a voltage-insensitive conductance, an instantaneous current (Macri and Accili 2004; Proenza et al. 2002). If the expression of a voltage-sensitive g_h is associated with a voltage-insensitive conductance in T and D stellate cells, then the magnitude of the voltage-insensitive, ZD7288-sensitive conductance would be expected to be related to the voltage-sensitive conductance. Figure 6*C* shows that it was the case in T stellate cells, and perhaps also in D stellate cells, that the magnitude of the voltage-insensitive ZD7288-sensitive instantaneous conductance is proportional to the $g_{h\ max}$ in stellate cells. Whether the voltage-insensitive Cs^+-sensitive conductance follows the same pattern was unclear (because the spread of $g_{h\ max}$ in our sample of recorded neurons was not wide enough). However, Fig. 6*A* implies that the voltage-insensitive, ZD7288-sensitive conductance is also proportional to g_{input} and that its expression may simply be related to the surface area of the cell.

Kinetics of I_h activation and deactivation

The activation and deactivation kinetics of I_h in T and D stellate cells are compared in Fig. 7. I_h activated more rapidly in D than in T stellate cells (Fig. 7A). The time course of the activation of currents was well described by the sum of two exponentials, the fast and slow time constants, τ_f and τ_s, which were voltage-dependent and in the tens and hundreds of milliseconds, respectively. Not only were each of the time con-

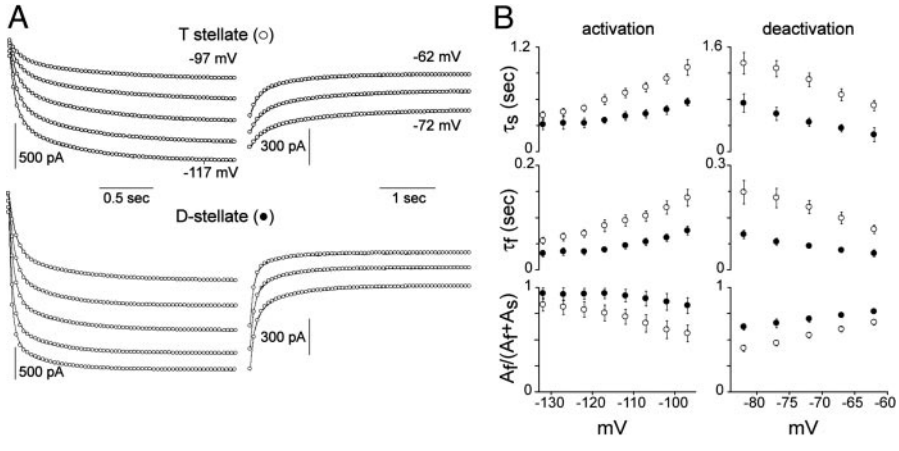

FIG. 7. Activation and deactivation kinetics of I_h in stellate neurons are voltage dependent. *A*: activation of I_h (—) is shown in responses to steps between –97 and –117 mV from a holding potential of –62 mV. Deactivation of I_h is illustrated in the tail currents after the voltage was returned from a fully activating pulse to –62, –67, or –72 mV. Superimposed on these recordings in a T stellate (*top*) and a D stellate cell (*bottom*) are fits with the sum of 2 exponential functions (○). The 1st 12–15 ms of the recorded current were excluded to avoid contamination of the fits by the capacitative currents. *B*: slow (τ_s, *top*) and fast (τ_f, *middle*) time constants for the activation (mean ± SE: $n = 8$ T stellate cells, ○; $n = 7$ D stellate cells, ●) and deactivation of I_h ($n = 6$ T stellate cells, $n = 4$ D stellate cells). *Bottom*: all time constants are voltage-dependent and are faster in D stellate than T stellate cells; the faster time constant (A_f) accounted for the majority of amplitude.

stants significantly faster, but also the relative contribution of the fast time constant was greater in D than in T stellate cells. For instance, in response to a voltage step to −97 mV, τ_f was 137 ± 16 ms in T stellate cells (n = 8) and 75 ± 9 ms in D stellate cells (n = 7); in the same cells τ_s was 966 ± 89 ms and 567 ± 45 ms in T and D stellate cells. The time constants became shorter with increasing hyperpolarization (Fig. 7*B*). The deactivation of I_h was examined by fitting double-exponential functions to the decay of the tail currents. After pulses to −122 mV that were long enough for the current to reach steady state, steps to between −62 and −82 mV caused I_h to deactivate. Deactivation kinetics were voltage-dependent and were significantly faster in D stellate than T stellate neurons. When the voltage was returned to near rest (−67 mV), the fast components (τ_f) were 148 ± 17 ms and 56 ± 7 and slow components (τ_s) were 866 ± 93 ms and 356 ± 57 in T (n = 6) and D (n = 4) stellate neurons, respectively, and the fast components were more dominant in D than T stellate neurons.

I_h contribution to stellate cells' excitability

To gain an understanding of how ZD7288- and Cs^+-sensitive currents affect the excitability of stellate cells, we compared the T and D stellate cells' behavior in current clamp in the absence and presence of these blockers. 50 μM ZD7288 and 2 mM Cs^+ hyperpolarized T and D stellate cells, increased their input resistance, abolished the sag in the voltage response, and prevented action potentials at the end of hyperpolarizing current steps (Fig. 8). Figure 8*A* shows that application of 50 μM ZD7288 to a T stellate cell increased the input resistance from 45 to 124 MΩ and induced a hyperpolarization of 10 mV; injecting 40 pA of positive current brought the resting potential at the cell body to its original level. Figure 8*B* shows that 2 mM Cs^+ increased the input resistance from 70 to 102 MΩ in a D stellate cell; the 3-mV hyperpolarization of the resting potential could be compensated by 10 pA. On average, 50 μM ZD7288 increased the input resistance in T stellate cells from 69 ± 5 to 130 ± 12 MΩ and hyperpolarized the resting potential by 8 ± 2 mV (n = 5). In D stellate cells, ZD7288 increased the input resistance from 96 ± 10 to 167 ± 12 MΩ and hyperpolarized the resting potential by 4 ± 1 mV (n = 3). In T stellate cells, 2 mM Cs^+ increased the input resistance from 86 ± 5 to 131 ± 17 MΩ and hyperpolarized the resting potential by 3.2 ± 0.7 mV (n = 3). Both ZD7288 and Cs^+ hyperpolarize the resting potential, indicate that they block a net depolarizing current; ZD7288 hyperpolarizes the resting potential significantly more than Cs^+.

The shapes of action potentials were altered by 50 μM ZD7288 or 2 mM Cs^+ (Fig. 8, *A* and *B*). Less current was required to bring cells to threshold in the presence of both blockers. Action potentials were broader and the first, fast undershoot following the action potential was less deep when I_h was blocked. In the presence of 50 μM ZD7288, large depolarizing currents generated a few action potentials at the onset of the pulse the peaks of which became progressively lower and eventually cells ceased firing (Fig. 8*A*). In the presence of Cs^+, failure to generate action potentials was less pronounced than in ZD7288 but was evident when cells fired at high frequencies.

In the presence of blockers of I_h or I_{hg} ZD7288 or Cs^+, two repolarizing components were clearly visible after action potentials, much like those illustrated for a D stellate cell in Fig. 1. Presumably the increased input resistance in the presence of ion channel blockers made voltage changes by small currents more prominent. Under control conditions, the voltage always rises monotonically after an action potential in T stellate cells, whereas double undershoots are observed in D stellate cells, characteristics that have served to distinguish these two types of cells (Fig. 1) (Fujino and Oertel 2001; Oertel et al. 1990). These results show that differences in the repolarization of action potentials in T and D stellate cells arise from differences

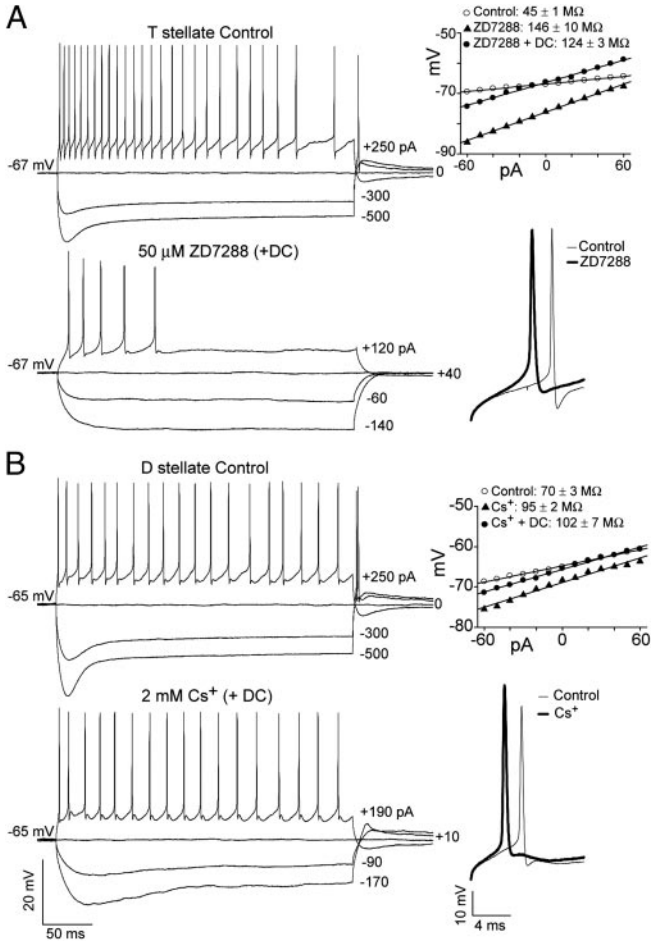

FIG. 8. ZD7288 and Cs^+ alter the firing patterns and the shapes of action potentials in stellate cells. *A*: in the presence of blockers of synaptic inputs, the T stellate neuron had a resting potential of −67 mV, fired a train of action potentials that adapted slightly (*top left*). Application of ZD7288 hyperpolarized the cell to −76 mV, eliminated the sag in responses to hyperpolarization and increased its input resistance (*right*). The membrane potential was returned to −67 mV with +40-pA DC current (*bottom left*). Depolarizing pulses evoked firing only at the onset of the pulse with action potentials that were followed by double undershoots; stronger current pulses did not overcome the firing block. *Inset at right*: action potentials with and without ZD7288; both were the first in a train elicited by a current step of +120 pA. Action potentials were broader and undershoots shallower in the presence of ZD7288 (thick trace). *B*: in a D stellate neuron, Cs^+ shifted the resting potential from −65 to −68 mV that was compensated with +10-pA of DC current (*bottom left*). Slope of voltage-current relationship document the increase in input resistance caused by 2 mM Cs^+ that it is not altered by returning the resting potential to its original level (*plot at right*). First action potentials in a train evoked by +120-pA current steps before (thin) and after (thick) addition of Cs^+ (*bottom right traces*). In the presence of Cs^+, action potentials were taller and had smaller fast undershoots and larger slow undershoots. All experiments were done in the presence of DNQX and strychnine to block spontaneous synaptic inputs.

in the relative magnitudes of the currents rather than from their presence or absence.

Modulation of I_h

One of the properties of I_h that makes it biologically interesting is that it can be modulated by changes in intracellular levels of cAMP (Robinson and Siegelbaum 2003). The observation that the voltage range of activation of I_h in octopus cells, cells that lie immediately adjacent to stellate cells, was not affected by cyclic nucleotides (Bal and Oertel 2000) raised the question whether I_h in stellate cells is modulated by cAMP. As in the previous study, modulation of I_h in stellate neurons was examined by perfusing a membrane-permeable analogue of cAMP, 8-Br-cAMP, in the bath. Both the voltage sensitivity and the kinetics of I_h in stellate cells were affected by 8-Br-cAMP.

In every T and D stellate cell tested ($n = 8$), the voltage-activation curve shifted in the depolarizing direction on addition of 8-Br-cAMP. Figure 9 shows an example of the action of 500 μM 8-Br-cAMP on a T stellate cell and 100 μM 8-Br-cAMP on a D stellate cell. The negative shift in the holding current at −62 mV reveals the activation of a depolarizing current. At 100 μM, 8-Br-cAMP caused a shift in the half-activation voltage ($V_{0.5}$) of I_h of 4.2 ± 1.0 mV ($n = 3$) in T stellate cells and 6.7 ± 0.4 mV ($n = 2$) in D stellate cells. The effect of 8-Br-cAMP was concentration-dependent; in T stellate cells 500 μM 8-Br-cAMP shifted $V_{0.5}$ by 11.7 ± 1.4 mV ($n = 4$).

In the presence of 8-Br-cAMP, activation of I_h was accelerated and deactivation was slowed. Changes in the kinetics of I_h that were observed in all T and D stellate cells tested are illustrated in a D stellate cell in the presence of 500 μM 8-Br-cAMP in Fig. 10. Activation by a pulse to –97 mV proceeded with time constants $\tau_s = 1050$ ms and $\tau_f = 148$ ms

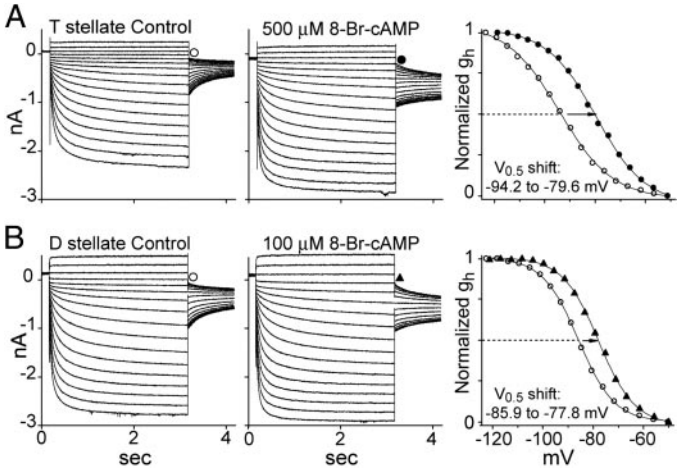

FIG. 9. 8-Br-cAMP modulates the voltage dependence of g_h in stellate cells. Voltage-clamp recordings were made of I_h in T stellate (*A*) or in a D stellate neuron (*B*) under control conditions (*left*) and after 8-Br-cAMP was added to the bath (*middle*). Neurons were held at −62 mV, then stepped to conditioning voltages between –52 and –132 mV for 3 s, and finally stepped to –77 mV. The plots (*right*) compare the voltage dependence of g_h, derived from tail currents as in Fig. 4, in the absence (○) and presence (●, ▲) of 8-Br-cAMP. Lines are fits to the Boltzmann equation. 500 μM 8-Br-cAMP shifted the $V_{0.5}$ from –94.2 (k = 10.5 mV) to –79.6 mV (k = 9.7 mV) in a T stellate cell (*A*); 100 μM 8-Br-cAMP shifted the $V_{0.5}$ from –85.9 mV ($k = 7.1$ mV) to –77.8 mV ($k = 7.2$ mV) in a D stellate cell.

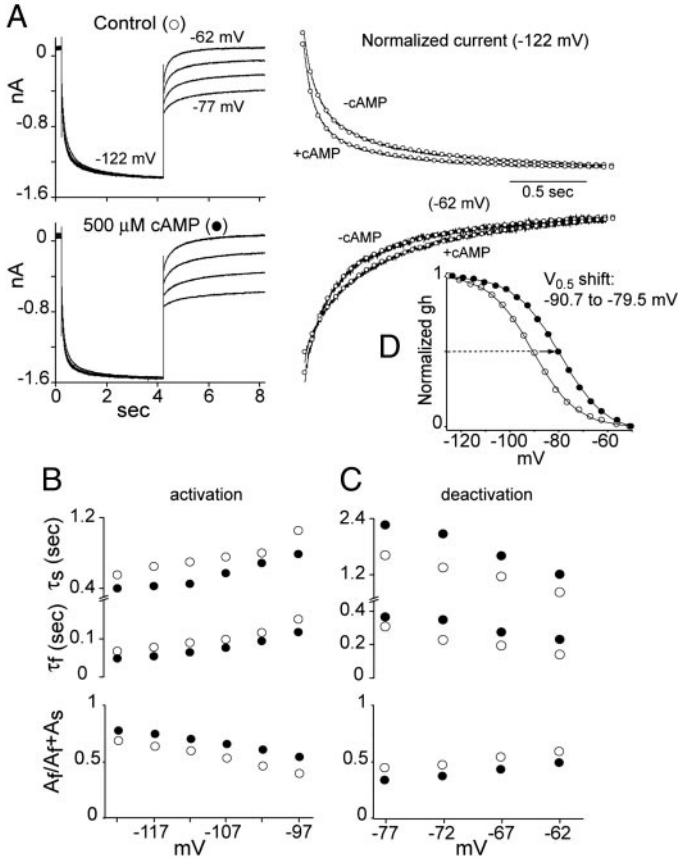

FIG. 10. 8-Br-cAMP modulates the kinetics of activation and deactivation of I_h. *A*: activation and deactivation were compared in the presence and absence of 500 μM 8-Br-cAMP in a D stellate cell. From a holding potential of −62 mV, a pulse to −122 mV activated I_h fully, and then deactivation was induced to voltages between –62 and –77 mV (*left*). The time course of activation was compared with averaged currents at –122 mV normalized to the steady-state current at an expanded time scale (*top right*). Time course of deactivation was compared after the voltage was stepped from –122 to −62 mV (*bottom right*). Superimposed on these currents are fits of the sum of 2 exponential functions (○). *B*: in the presence of 8-Br-cAMP (●), I_h activated faster and the contribution of the fast component was larger than under control conditions (○). *C*: in the presence of 8-Br-cAMP (●), deactivation slowed; the fast time constant was slower and its contribution was smaller. *D*: 8-Br-cAMP shifted the voltage range of activation by 11 mV in the depolarizing direction. Boltzmann fits show that the $V_{0.5}$ shifted from –90.7 to –79.5 mV; slope factors were 8.9 mV, control and 9.3 mV, presence of 8-Br-cAMP.

in control conditions and $\tau_s = 784$ and $\tau_f = 116$ ms in the presence of 8-Br-cAMP with the fast component being more prominent (Fig. 10*B*). Deactivation time constants slowed and the slower component increased in prominence in the presence of 8-Br-cAMP (Fig. 10*C*). In this cell, the voltage range of activation of I_h shifted by 11.2 mV in the presence of 8-Br-cAMP (Fig. 10*D*).

Influence of temperature on I_h

Changes in temperature affected the kinetics and the magnitude of I_h in stellate neurons (Fig. 11). Lowering the temperature from 33 to 27°C reduced the amplitude of the evoked inward current as well as the rates of activation and deactivation. The changes in amplitude of I_h in this cell, as in all others tested, were stable over the 12 min over which it was monitored. The reduction in temperature did not alter the voltage

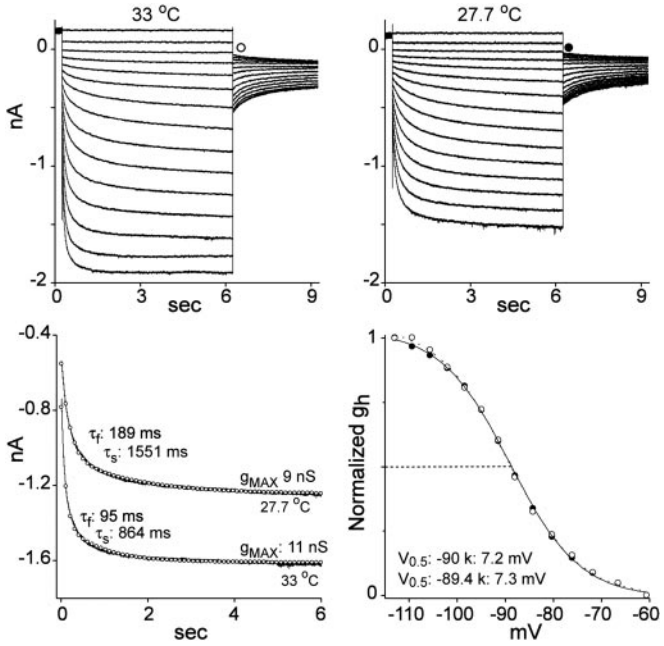

FIG. 11. Temperature affects the amplitude, kinetics, and voltage dependence of I_h. A T stellate cell was held at −62, stepped to between −62 and −127 mV and then returned to −77 mV. Currents were first recorded at the normal temperature, 33°C (*top left*). The temperature was then reduced to 27°C and I_h was recorded ~8 min later (*top right*). Currents in responses to a step to −122 mV at the two temperatures were fitted with double-exponential functions (○). τ_f and τ_s, represent the fast and slow exponential components and g_h the conductance at the steady state (*bottom left*). The tail currents shown in *A* and *B* were used to compare the voltage dependence of g_h at the 2 temperatures. Fits to the Boltzmann function showed that there was no difference between them: at 33°C, $V_{0.5}$ = −89.4 mV and k = 7.3 mV and at 27°C $V_{0.5}$ = –90 and k = 7.2 mV (*bottom right*).

dependence of activation; in T stellate cells $V_{0.5}$ was −91 ± 1.6 at 33°C and −90 ± 2.0 at 27°C (n = 5). In T stellate cells $g_{h\ max}$ was reduced with a Q_{10} 1.3 ± 0.05 and the fast activation time constant was slowed with a Q_{10} 3.3 ± 0.3 when the temperature was reduced from 33 to 27°C (n = 6).

DISCUSSION

Hyperpolarization-activated conductances are common in neurons even though the voltage range of activation spans membrane potentials that are largely beyond the physiological range. The present experiments show that g_h, the voltage sensitivity of which is regulated through cAMP, affects the excitability of stellate neurons by its influence on the resting potential and on the input conductance. In making measurements in T and D stellate cells that were sufficiently detailed to illustrate how consistent certain features of g_h are among neurons and also how other features of g_h seem to be tailored to suit different types of neurons in the VCN, we found unexpectedly that these cells also have a voltage-insensitive, ZD7288-sensitive, and Cs^+-sensitive conductances that are 5–10 times larger than g_h at −62 mV and the magnitude of which is proportional to these cells' maximum g_h.

Characteristics of I_h in neurons from the VCN

I_h reverses at approximately –40 mV in both T and D stellate cells. In other cells, too, reversal potentials of this mixed cation current generally lie between –30 and –44 mV (Bal and Oertel 2000; Banks et al. 1993; Chen 1997; Maccaferri and McBain 1996; McCormick and Pape 1990b; Mo and Davis 1997; Saitow and Konishi 2000; Spain et al. 1987). This reversal potential reflects a permeability ratio P_{Na}/P_K of ~0.3 (Wollmuth and Hille 1992). The $g_{h\ max}$ of stellate cells, ~20 nS in T and ~30 nS in D stellate cells, was considerably smaller than that in octopus cells (~150 nS) and the half-activation voltages around −88 mV were more hyperpolarized than that measured in octopus cells (approximately −65 mV) (Bal and Oertel 2000). The differing maximal conductances and voltage ranges of activation result in large differences in the resting g_h. On average only ~4% $g_{h\ max}$, is activated in T and D stellate cells at rest, whereas 62 nS g_h, 41% of $g_{h\ max}$, is activated in octopus cells (Bal and Oertel 2000). The kinetics of I_h is more rapid in D stellate than in T stellate cells, and both are slower than in octopus cells. In each of the cells, τ_{fast} dominates the time course of the activation of I_h. Currents evoked by steps from −62 mV to the voltage where g_h was about half-maximally activated had a τ_{fast} of 50 ms (−67 mV) in octopus cells, 140 ms (−97 mV) in T stellate, and 75 ms (−97 mV) in D stellate cells. For the same voltage steps, τ_{slow} was 190 ms in octopus, 960 ms in T stellate, and 560 ms in D stellate cells. Bushy cells express g_h with characteristics generally similar to those described here for stellate neurons; measurements in bushy cells are not directly comparable because they were made from younger animals and at lower temperatures (Cuttle et al. 2001); the expression and possibly the voltage dependence of I_h are developmentally regulated in bushy cells as in other cell types (Cuttle et al. 2001; Tanaka et al. 2003).

A characteristic feature of g_h is that its biophysical properties are regulated by cAMP. In T and D stellate cells, 8-Br-cAMP shifted its voltage dependence in the depolarizing direction. Increases in intracellular cAMP shift the voltage range of activation in the depolarizing direction with little or no change in $g_{h\ max}$ in many cell types including bushy cells (Banks et al. 1993; Cathala and Paupardin-Tritsch 1999; Chen et al. 2001; Cuttle et al. 2001; DiFrancesco and Tortora 1991; Ingram and Williams 1996; Ludwig et al. 1998; McCormick and Pape 1990b; Saitow and Konishi 2000; Santoro and Tibbs 1999; Santoro et al. 1998; Tokimasa and Akasu 1990; Vargas and Lucero 1999). The maximal shift is related to the type of channels that form I_h and also to the amount of basal modulation by the resting levels of cAMP (Chen et al. 2001). In octopus cells, g_h seems not to be modulated in similar experiments (Bal and Oertel 2000), suggesting that in these cells, I_h channels are either fully modulated or that they are formed largely from subunits whose sensitivity to cAMP is small. In octopus cells, the magnitude of I_h also changes with temperature and then adapts over tens of minutes (Cao and Oertel 2005). We did not observe such adaptation in T or D stellate cells.

Possible molecular identity of I_h in neurons from the VCN

I_h is mediated through hyperpolarization-activated cyclic nucleotide-gated (HCN) channels. Four subunits, HCN1-HCN4, form these channels (Ludwig et al. 1998; Santoro and Tibbs 1999; Santoro et al. 1997, 1998). Homomeric channels expressed in heterologous expression systems have differing voltage sensitivity, kinetics, and sensitivity to cyclic nucleo-

tides. Channels of HCN1 subunits are fastest, HCN2 channels activate and deactivate at intermediate rates, and HCN4 channels are the slowest (Moosmang et al. 2001). HCN1 are less sensitive to cyclic nucleotide modulation than the others (Santoro et al. 1998; Ulens and Tytgat 2001), whereas HCN2 is more sensitive to cAMP (Chen et al. 2001). HCN subunits also combine to form heteromeric channels (Altomare et al. 2003; Chen et al. 2001; Ulens and Tytgat 2001).

The protein of HCN1 and HCN2 subunits has been detected in the octopus cell area and in adjacent regions where T and D stellate cells are located (Koch et al. 2004). The observed properties indicate that stellate neurons seem preferentially to express the relatively slow and modulatable HCN2 subunits. On the other hand, the fast kinetics, depolarized voltage range of activation, and apparent insensitivity to cAMP indicate that HCN1 is the most prevalent subunit expressed in octopus cells. Measurements of the levels of mRNA expression in the VCN also indicate that HCN1 and HCN2 are the most commonly expressed subunits (Santoro et al. 2000).

Assessment of three methods for isolating I_h

In our experiments, I_h was isolated by widely used electrophysiological and pharmacological techniques, its voltage sensitivity, ZD7288 sensitivity, and Cs^+ sensitivity. It was surprising that the ZD7288-sensitive and Cs^+-sensitive conductances were so much greater than the estimate of g_h from the Boltzmann relationship (Fig. 6*B*).

It has long been known that I_h is sensitive to extracellular Cs^+ (Maccaferri et al. 1993; McCormick and Pape 1990b; Spain et al. 1987). In the present experiments, 2 mM Cs^+ blocked a conductance that was about sixfold greater than the voltage-sensitive g_h but about half as great as that blocked by 50 μM ZD7288 at −62 mV in T stellate cells. In the MNTB, Cs^+ also blocked a larger conductance at rest than expected from the Boltzmann analysis (Banks et al. 1993). The block may not have been complete or entirely specific. The block of I_h by Cs^+ is known to be more complete at hyperpolarized than at depolarized voltages; for example, at −62 mV, only 60% of heterologously expressed HCN2 channels were blocked by 5 mM Cs^+ (DiFrancesco 1982; Moroni et al. 2000). There is also the possibility that Cs^+ is not entirely specific for inwardly rectifying mixed cation channels; it could, for example, affect inwardly rectifying K^+ channels (Lesage et al. 1995; Mermelstein et al. 1998). In stellate cells, extracellular Cs^+ at 2 mM seems to block primarily g_h because its application causes the resting potentials to hyperpolarize. The present results are consistent with the conclusion that Cs^+ blocks the voltage-sensitive g_h as well as a voltage-insensitive conductance but that the block is incomplete.

ZD7288 has been widely used to test the action of I_h because it is considered to block this current nearly completely and with considerable specificity (BoSmith et al. 1993). This drug has been used to assay I_h in octopus cells of the VCN (Bal and Oertel 2000), substantia nigra neurons (Harris and Constanti 1995), CA1 hippocampal pyramidal cells (Gasparini and DiFrancesco 1997; Macaferri and McBain 1996), thalamic neurons (Luthi et al. 1998), and cerebellar basket cells (Saitow and Konishi 2000). In hippocampal CA1 neurons, the half-maximal blocking of I_h required 10.5 μM, and at 50 μM, the concentration used in the present experiments, the block was nearly saturated (Gasparini and DiFrancesco 1997). At 50 μM, ZD7288 has been reported to block glutamate receptors of both AMPA and *N*-methyl-D-aspartate (NMDA) subtypes (Chen 2004) and a low-voltage-activated Ca^{2+} conductance (Felix et al. 2003), but these conductances were blocked by DNQX and by voltage, respectively, in our experiments. In hippocampal pyramidal cells and in thalamic relay neurons, neither Na^+- nor Ca^{2+}-dependent action potentials were affected by ZD7288 (Gasparini and DiFrancesco 1997; Luthi et al. 1998; Maccaferri and McBain 1996). Furthermore, the removal of Ca^{2+} does not affect the resting potential or the shape of action potentials in T stellate cells (Wickesberg and Oertel 1989), indicating that voltage-sensitive Ca^{2+} conductances are small. It thus seems unlikely that the block of these conductances accounts for the unexpectedly large-conductance block by ZD7288 near rest.

An interesting possibility is that ZD7288 blocks a voltage-insensitive current that is mediated through HCN channels. Accili and his colleagues have suggested that the expression of HCN2 channels is associated with the expression of an "instantaneous current" that is voltage insensitive over the tested voltage range and the magnitude of which is directly proportional to the amount of heterologously expressed HCN protein and that increased on coexpression with the regulatory subunit minK-related peptide 1 (Macri and Accili 2004; Proenza et al. 2002). These authors concluded that HCN channels mediate a voltage-insensitive, instantaneous current through leaky channels. In contrast to the present results, the instantaneous current was insensitive to extracellular Cs^+, but its sensitivity to ZD7288 was not reported. In hippocampal pyramidal cells ZD7288, at 10–20 μM, blocked ~18% of the resting conductance (Gasparini and DiFrancesco 1997). Other authors, however, did not observe an instantaneous, ZD7288-sensitive conductance in thalamic relay neurons (Luthi et al. 1998) and with coexpression of HCN with the MiRP1 protein in cardiac sinoatrial cells (Qu et al. 2004).

Boltzmann analyses of conductances activated and deactivated by voltage are also subject to errors. First, if the conditioning pulses are too short, activation can be underestimated especially for voltage pulses that activate the conductance slowly. Our tests suggest this was not a significant problem when the pulses were ≥3 s. Second, the voltage range over which g_h-*V* curves were measured should be wide enough for activation and deactivation to be saturated. The range of activation used, –50 and –125 mV, was generally wide enough to include saturation (Fig. 4). Third, with imperfect space-clamping, the slope of the g_h-*V* function can appear less steep than it is. One indication that g_h was reasonably well space-clamped is that plots of the chord conductances were linear and intersected at one point (Fig. 3). It is unlikelly that the small errors in the g_h-*V* curves in our measurements can underly the large difference in resting activation of g_h and resting ZD7288 and Cs^+ sensitivity, indicating that 50 μM ZD7288 and 2 mM Cs^+ block a voltage-insensitive conductance in addition to g_h.

Factors that determine the excitability of T and D stellate cells

The electrical excitability of T and D stellate cells is sensitive to small changes in resting potential and resting conductance. The resting potentials of the T and D stellate cells recorded here in parasagittal slices were on average 5 mV more

negative and the input resistances lower by more than a factor of two than those recorded from coronal slices (Fujino and Oertel 2001). These results suggest that processes of stellate cells have a greater tendency to be cut in coronal than parasagittal slices, a conclusion consistent with the morphology of these cells (Oertel et al. 1990). These results also suggest that the resting potential at the cell body is hyperpolarized by the presence of these processes.

Several conductances have been identified that contribute to setting the resting potential of stellate cells. Of the resting conductances, ~15 nS in both types of stellate cells, ~20% is blocked by 2 mM 4-AP. 4-AP blocks low-voltage-activated K^+ conductances (Bal and Oertel 2001; Banks et al. 1993; Brew and Forsythe 1995; Manis and Marx 1991; Rathouz and Trussell 1998; Rothman and Manis 2003; Wu 1999) and a small proportion of g_h (Bal and Oertel 2000; present experiments). The present experiments show that the voltage-sensitive g_h accounts for ~10% of the input conductance and that the voltage-insensitive, ZD7288-sensitive conductance contributes roughly another 20%. A muscarine-sensitive, voltage-insensitive conductance of ~1 nS affects T stellate, but not D stellate, cells (Fujino and Oertel 2001).

The present experiments also reveal the importance of the input conductance in the generation of action potentials. Increasing the input resistance with ZD7288 or Cs^+ weakens or prevents firing. In the presence of these blockers, action potentials become broader and their peaks become lower with repeated firing, presumably because slower depolarization results in greater inactivation of Na^+ currents. By increasing the input conductance at rest, ZD7288- and Cs^+-sensitive conductances promote rapid firing in stellate cells.

ACKNOWLEDGMENTS

M. J. McGinley, X. Cao, and P. Poon read the manuscript critically more than once, debated its intricacies, and made thoughtful suggestions for which we are indeed grateful. We are lucky to have had help from I. Siggelkow, S. Shatadal, and R. Kochhar.

GRANTS

The work was supported by National Institute of Deafness and Other Communications Disorders Grant DC-00176.

REFERENCES

Adams JC and Warr WB. Origins of axons in the cat's acoustic striae determined by injection of horseradish peroxidase into severed tracts. *J Comp Neurol* 170: 107–122, 1976.

Altomare C, Terragni B, Brioschi C, Milanesi R, Pagliuca C, Viscomi C, Moroni A, Baruscotti M, and DiFrancesco D. Heteromeric HCN1-HCN4 channels: a comparison with native pacemaker channels from the rabbit sinoatrial node. *J Physiol* 549: 347–359, 2003.

Arnott RH, Wallace MN, Shackleton TM, and Palmer AR. Onset neurones in the anteroventral cochlear nucleus project to the dorsal cochlear nucleus. *J Assoc Res Otolaryngol* 5: 153–170, 2004.

Bal R and Oertel D. Hyperpolarization-activated, mixed-cation current (I_h) in octopus cells of the mammalian cochlear nucleus. *J Neurophysiol* 84: 806–817, 2000.

Bal R and Oertel D. Potassium currents in octopus cells of the mammalian cochlear nuclei. *J Neurophysiol* 86: 2299–2311, 2001.

Banks MI, Pearce RA, and Smith PH. Hyperpolarization-activated cation current (I_h) in neurons of the medial nucleus of the trapezoid body: voltage-clamp analysis and enhancement by norepinephrine and cAMP suggest a modulatory mechanism in the auditory brain stem. *J Neurophysiol* 70: 1420–1432, 1993.

Blackburn CC and Sachs MB. Classification of unit types in the anteroventral cochlear nucleus: PST Histograms and regularity analysis. *J Neurophysiol* 62: 1303–1329, 1989.

BoSmith RE, Briggs I, and Sturgess NC. Inhibitory actions of ZENECA ZD7288 on whole-cell hyperpolarization activated inward current (I_f) in guinea pig dissociated sinoatrial node cells. *Br J Pharmacol* 110: 343–349, 1993.

Brew HM and Forsythe ID. Two voltage-dependent K^+ conductances with complementary functions in postsynaptic integration at a central auditory synapse. *J Neurosci* 15: 8011–8022, 1995.

Cant NB. The fine structure of two types of stellate cells in the anterior division of the anteroventral cochlear nucleus of the cat. *Neurosci* 6: 2643–2655, 1981.

Cant NB and Gaston KC. Pathways connecting the right and left cochlear nuclei. *J Comp Neurol* 212: 313–326, 1982.

Cao X-J and Oertel D. Temperature affects voltage-sensitive conductances differentially in octopus cells of the mammalian cochlear nucleus. *J Neurophysiol* 94: 821–832, 2005.

Cathala L and Paupardin-Tritsch D. Effect of catecholamines on the hyperpolarization-activated cationic I_h and the inwardly rectifying potassium *I*(Kir) currents in the rat substantia nigra pars compacta. *Eur J Neurosci* 11: 398–406, 1999.

Chen C. Hyperpolarization-activated current (I_h) in primary auditory neurons. *Hear Res* 110: 179–190, 1997.

Chen C. ZD7288 inhibits postsynaptic glutamate receptor-mediated responses at hippocampal perforant path-granule cell synapses. *Eur J Neurosci* 19: 643–649, 2004.

Chen S, Wang J, and Siegelbaum SA. Properties of hyperpolarization-activated pacemaker current defined by coassembly of HCN1 and HCN2 subunits and basal modulation by cyclic nucleotide. *J Gen Physiol* 117: 491–503, 2001.

Cuttle MF, Rusznak Z, Wong AY, Owens S, and Forsythe ID. Modulation of a presynaptic hyperpolarization-activated cationic current (*I*(h)) at an excitatory synaptic terminal in the rat auditory brain stem. *J Physiol* 534: 733–744, 2001.

DiFrancesco D. Block and activation of the pacemaker if channel in calf Purkinje fibers: effects of potassium, caesium and rubidium. *J Physiol* 329: 485–507, 1982.

DiFrancesco D, and Tortora P. Direct activation of cardiac pacemaker channels by intracellular cyclic AMP. *Nature* 351: 145–147, 1991.

Doan TN and Kunze DL. Contribution of the hyperpolarization-activated current to the resting membrane potential of rat nodose sensory neurons. *J Physiol* 514: 125–138, 1999.

Doucet JR and Ryugo DK. Projections from the ventral cochlear nucleus to the dorsal cochlear nucleus in rats. *J Comp Neurol* 385: 245–264, 1997.

Felix R, Sandoval A, Sanchez D, Gomora JC, De la Vega-Beltran JL, Trevino CL, and Darszon A. ZD7288 inhibits low-threshold Ca^{2+} channel activity and regulates sperm function. *Biochem Biophys Res Comm* 311: 187–192, 2003.

Ferragamo MJ, Golding NL, and Oertel D. Synaptic inputs to stellate cells in the ventral cochlear nucleus. *J Neurophysiol* 79: 51–63, 1998.

Ferragamo MJ and Oertel D. Octopus cells of the mammalian ventral cochlear nucleus sense the rate of depolarization. *J Neurophysiol* 87: 2262–2270, 2002.

Fujino K and Oertel D. Cholinergic modulation of stellate cells in the mammalian ventral cochlear nucleus. *J Neurosci* 21: 7372–7383, 2001.

Gasparini S and DiFrancesco D. Action of the hyperpolarization-activated current (I_h) blocker ZD7288 in hippocampal CA1 neurons. *Pfluegers* 435: 99–106, 1997.

Golding NL, Robertson D, and Oertel D. Recordings from slices indicate that octopus cells of the cochlear nucleus detect coincident firing of auditory nerve fibers with temporal precision. *J Neurosci* 15: 3138–3153, 1995.

Harris NC and Constanti A. Mechanism of block by ZD 7288 of the hyperpolarization-activated inward rectifying current in guinea pig substantia nigra neurons in vitro. *J Neurophysiol* 74: 2366–2378, 1995.

Ingram SL and Williams JT. Modulation of the hyperpolarization-activated current (I_h) by cyclic nucleotides in guinea-pig primary afferent neurons. *J Physiol* 492: 97–106, 1996.

Jiang D, Palmer AR, and Winter IM. Frequency extent of two-tone facilitation in onset units in the ventral cochlear nucleus. *J Neurophysiol* 75: 380–395, 1996.

Koch U, Braun M, Kapfer C, and Grothe B. Distribution of HCN1 and HCN2 in rat auditory brain stem nuclei. *Eur J Neurosci* 20: 79–91, 2004.

Kossl M and Vater M. Noradrenaline enhances temporal auditory contrast and neuronal timing precision in the cochlear nucleus of the mustached bat. *J Neurosci* 9: 4169–4178, 1989.

Lesage F, Guillemare E, Fink M, Duprat F, Heurteaux C, Fosset M, Romey G, Barhanin J, and Lazdunski M. Molecular properties of neuronal G-protein-activated inwardly rectifying K^+ channels. *J Biol Chem* 270: 28660–28667, 1995.

Ludwig A, Zong X, Jeglitsch M, Hofmann F, and Biel M. A family of hyperpolarization-activated mammalian cation channels. *Nature* 393: 587–591, 1998.

Luthi A, Bal T, and McCormick DA. Periodicity of thalamic spindle waves is abolished by ZD7288, a blocker of I_h. *J Neurophysiol* 79: 3284–3289, 1998.

Maccaferri G, Mangoni M, Lazarri A, and DiFrancesco D. Properties of hyperpolarization-activated current in rat hippocampal pyramidal cells. *J Neurophysiol* 69: 2129–2136, 1993.

Maccaferri G and McBain CJ. The hyperpolarization-activated current (I_h) and its contribution to pacemaker activity in rat CA1 hippocampal stratum oriens-alveus interneurones. *J Physiol* 497: 119–130, 1996.

Macri V and Accili EA. Structural elements of instantaneous and slow gating in hyperpolarization-activated cyclic nucleotide-gated channels. *J Biol Chem* 279: 16832–16846, 2004.

Magee JC. Dendritic hyperpolarization-activated currents modify the integrative properties of hippocampal CA1 pyramidal neurons. *J Neurosci* 18: 7613–7624, 1998.

Manis PB and Marx SO. Outward currents in isolated ventral cochlear nucleus neurons. *J Neurosci* 11: 2865–2880, 1991.

McCormick DA and Pape HC. Noradrenergic and serotonergic modulation of a hyperpolarization-activated cation current in thalamic relay neurons. *J Physiol* 431: 319–342, 1990a.

McCormick DA and Pape HC. Properties of a hyperpolarization-activated cation current and its role in rhythmic oscillation in thalamic relay neurons. *J Physiol* 431: 291–318, 1990b.

Mermelstein PG, Song WJ, Tkatch T, Yan Z, and Surmeier DJ. Inwardly rectifying potassium (IRK) currents are correlated with IRK subunit expression in rat nucleus accumbens medium spiny neurons. *J Neurosci* 18: 6650–6661, 1998.

Mo ZL and Davis RL. Heterogeneous voltage dependence of inward rectifier currents in spiral ganglion neurons. *J Neurophysiol* 78: 3019–3027, 1997.

Moosmang S, Stieber J, Zong X, Biel M, Hofmann F, and Ludwig A. Cellular expression and functional characterization of four hyperpolarization-activated pacemaker channels in cardiac and neuronal tissues. *Eur J Biochem* 268: 1646–1652, 2001.

Moroni A, Barbuti A, Altomare C, Viscomi C, Morgan J, Baruscotti M, and DiFrancesco D. Kinetic and ionic properties of the human HCN2 pacemaker channel. *Pfluegers* 439: 618–626, 2000.

Needham K and Paolini AG. Fast inhibition underlies the transmission of auditory information between cochlear nuclei. *J Neurosci* 23: 6357–6361, 2003.

Nelken I and Young ED. Two separate inhibitory mechanisms shape the responses of dorsal cochlear nucleus type IV units to narrowband and wideband stimuli. *J Neurophysiol* 71: 2446–2462, 1994.

Oertel D, Bal R, Gardner SM, Smith PH, and Joris PX. Detection of synchrony in the activity of auditory nerve fibers by octopus cells of the mammalian cochlear nucleus. *Proc Nat Acad Sci USA* 97: 11773–11779, 2000.

Oertel D, Wu SH, Garb MW, and Dizack C. Morphology and physiology of cells in slice preparations of the posteroventral cochlear nucleus of mice. *J Comp Neurol* 295: 136–154, 1990.

Palmer AR, Jiang D, and Marshall DH. Responses of ventral cochlear nucleus onset and chopper units as a function of signal bandwidth. *J Neurophysiol* 75: 780–794, 1996.

Palmer AR and Winter IM. The temporal window of two-tone facilitation in onset units of the ventral cochlear nucleus. *Audiol Neurootol* 1: 12–30, 1996.

Pape HC. Queer current and pacemaker: the hyperpolarization-activated cation current in neurons. *Annu Rev Physiol* 58: 299–327, 1996.

Pedarzani P and Storm JF. Protein kinase A-independent modulation of ion channels in the brain by cyclic AMP. *Proc Natl Acad Sci USA* 92: 11716–11720, 1995.

Proenza C, Angoli D, Agranovich E, Macri V, and Accili EA. Pacemaker channels produce an instantaneous current. *J Biol Chem* 277: 5101–5109, 2002.

Qu J, Kryukova Y, Potapova IA, Doronin SV, Larsen M, Krishnamurthy G, Cohen IS, and Robinson RB. MiRP1 modulates HCN2 channel expression and gating in cardiac myocytes. *J Biol Chem* 279: 43497–43502, 2004.

Rathouz M and Trussell L. Characterization of outward currents in neurons of the avian nucleus magnocellularis. *J Neurophysiol* 80: 2824–2835, 1998.

Robinson RB and Siegelbaum SA. Hyperpolarization-activated cation currents: from molecules to physiological function. *Annu Rev Physiol* 65: 453–480, 2003.

Rothman JS and Manis PB. Differential expression of three distinct potassium currents in the ventral cochlear nucleus. *J Neurophysiol* 89: 3070–3082, 2003.

Saitow F and Konishi S. Excitability increase induced by beta-adrenergic receptor-mediated activation of hyperpolarization-activated cation channels in rat cerebellar basket cells. *J Neurophysiol* 84: 2026–2034, 2000.

Santoro B, Chen S, Luthi A, Pavlidis P, Shumyatsky GP, Tibbs GR, and Siegelbaum SA. Molecular and functional heterogeneity of hyperpolarization-activated pacemaker channels in the mouse CNS. *J Neurosci* 20: 5264–5275, 2000.

Santoro B, Grant SG, Bartsch D, and Kandel ER. Interactive cloning with the SH3 domain of N-src identifies a new brain specific ion channel protein, with homology to eag and cyclic nucleotide-gated channels. *Proc Natl Acad Sci USA* 94: 14815–14820, 1997.

Santoro B, Liu DT, Yao H, Bartsch D, Kandel ER, Siegelbaum SA, and Tibbs GR. Identification of a gene encoding a hyperpolarization-activated pacemaker channel of brain. *Cell* 93: 717–729, 1998.

Santoro B and Tibbs GR. The HCN gene family: molecular basis of the hyperpolarization-activated pacemaker channels. *Ann N Y Acad Sci* 868: 741–764, 1999.

Shin KS, Rothberg BS, and Yellen G. Blocker state dependence and trapping in hyperpolarization-activated cation channels: evidence for an intracellular activation gate. *J Gen Physiol* 117: 91–101, 2001.

Smith PH, Massie A, and Joris PX. Acoustic stria: anatomy of physiologically characterized cells and their axonal projection patterns. *J Comp Neurol* 482: 349–371, 2005.

Smith PH and Rhode WS. Structural and functional properties distinguish two types of multipolar cells in the ventral cochlear nucleus. *J Comp Neurol* 282: 595–616, 1989.

Spain WJ, Schwindt PC, and Crill WE. Anomalous rectification in neurons from cat sensorimotor cortex in vitro. *J Neurophysiol* 57: 1555–1576, 1987.

Tanaka S, Wu N, Hsaio CF, Turman J Jr, and Chandler SH. Development of inward rectification and control of membrane excitability in mesencephalic v neurons. *J Neurophysiol* 89: 1288–1298, 2003.

Tokimasa T and Akasu T. Cyclic AMP regulates an inward rectifying sodium-potassium current in dissociated bull-frog sympathetic neurons. *J Physiol* 420: 409–429, 1990.

Ulens C and Tytgat J. Functional heteromerization of HCN1 and HCN2 pacemaker channels. *J Biol Chem* 276: 6069–6072, 2001.

van Ginneken AC, and Giles W. Voltage clamp measurements of the hyperpolarization-activated inward current *I*(f) in single cells from rabbit sino-atrial node. *J Physiol* 434: 57–83, 1991.

Vargas G, Lucero MT. Dopamine modulates inwardly rectifying hyperpolarization-activated current (I_h) in cultured rat olfactory receptor neurons. *J Neurophysiol* 81: 149–158, 1999.

Wickesberg RE and Oertel D. Auditory nerve neurotransmitter acts on a kainate receptor: evidence from intracellular recordings in brain slices from mice. *Brain Res* 486: 39–48, 1989.

Williams SR and Stuart GJ. Site independence of EPSP time course is mediated by dendritic *I*(h) in neocortical pyramidal neurons. *J Neurophysiol* 83: 3177–3182, 2000.

Wollmuth LP and Hille B. Ionic selectivity of I_h channels of rod photoreceptors in tiger salamanders. *J Gen Physiol* 100: 749–765, 1992.

Wu SH. Physiological properties of neurons in the ventral nucleus of the lateral lemniscus of the rat: intrinsic membrane properties and synaptic responses. *J Neurophysiol* 81: 2862–2874, 1999.